Published in final edited form as:
Methods. 2014 March 15; 66(2): 200–207. doi:10.1016/j.ymeth.2013.06.017.

Measuring protein interactions using Förster resonance energy transfer and fluorescence lifetime imaging microscopy

Richard N. Day*
Department of Cellular and Integrative Physiology, Indiana University School of Medicine, 635 Barnhill Dr., Indianapolis, IN 46202 USA

Abstract

The method of fluorescence lifetime imaging microscopy (FLIM) is a quantitative approach that can be used to detect Förster Resonance Energy Transfer (FRET). The use of FLIM to measure the FRET that results from the interactions between proteins labeled with fluorescent proteins (FPs) inside living cells provides a non-invasive method for mapping interactomes. Here, the use of the phasor plot method to analyze frequency domain (FD) FLIM measurements is described, and measurements obtained from cells producing the 'FRET standard' fusion proteins are used to validate the FLIM system for FRET measurements. The FLIM FRET approach is then used to measure both homologous and heterologous protein-protein interactions (PPI) involving the CCAAT/enhancer-binding protein alpha (C/EBPα). C/EBPα is a transcription factor that controls cell differentiation, and localizes to heterochromatin where it interacts with the heterochromatin protein 1 alpha (HP1α). The FLIM-FRET method is used to quantify the homologous interactions between the FP-labeled basic leucine zipper (BZip) domain of C/EBPα. Then the heterologous interactions between the C/EBPa BZip domain and HP1a are quantified using the FRET-FLIM method. The results demonstrate that the basic region and leucine zipper (BZip) domain of C/EBPα is sufficient for the interaction with HP1α in regions of heterochromatin.

Keywords

fluorescence lifetime imaging microscopy (FLIM); Förster resonance energy transfer (FRET) microscopy; fluorescent proteins (FPs); protein-protein interactions (PPI)

1. Introduction

Cellular proteins function as components in larger protein complexes that are transiently assembled to mediate specific processes. The interconnected networks of protein-protein interactions (PPI) that form these complexes have dynamic properties and are typically localized to specific regions within the cell, reflecting the activity of the complex. The mapping of PPI networks in mammalian cells, known as interactomes, is a critical step towards understanding human disease processes. What is more, the mapping of interactomes provides the insights necessary for the development of therapeutic strategies designed to disrupt specific PPI linked to disease [1]. The high-throughput screening methods most often used for mapping PPI are yeast two-hybrid and co-affinity purification assays followed by

*Correspondence should be addressed to RND., Phone: 317 274 2166, rnday@iupui.edu.

mass spectrometry [2–4]. The information obtained from these screening methods is supplemented with information from curated interaction datasets derived from the literature [5], and from predictive computer algorithms [6].

A problem with these approaches is that it is difficult to separate biologically significant PPI from random interactions that may be detected by yeast two-hybrid, or non-specific interactions that can be detected in the disrupted cell preparations used for co-affinity purification. Protein interactions within cells are very dependent on the context in which they occur, and are dynamic and transient in nature. Therefore, some of the interactions mapped by these screening techniques may not be biologically relevant, and these approaches may fail to detect transient, but meaningful interactions that occur in specific cell-types. Furthermore, these approaches do not identify dynamic PPI that may only occur in discrete subcellular compartments. Hence, the interactome map developed by high throughput approaches still requires verification by many different types of cellular assays.

Most importantly, since many PPI are dependent upon the association with specific cellular components, verification of these types of interactions may only be possible within the context of the intact cell. Therefore, the development of non-invasive quantitative imaging techniques to visualize the protein interactions inside living cells is necessary for mapping the interactome. Here, a non-invasive imaging approach that enables the detection of PPI inside living cells is described. The approach involves the use of frequency domain fluorescence lifetime imaging microscopy (FD FLIM) to detect the Förster resonance energy transfer (FRET) that results from the interactions between proteins labeled with fluorescent proteins (FPs) inside living cells.

2. Materials and Methods

2.1. Expression plasmids and purified fluorescent proteins

The cDNA for Venus was obtained from Dr. Atsushi Miyawaki (RIKEN, Japan) [7]. The plasmids encoding the monomeric (m)Cerulean, mCerulean3, mTurquoise, and mTurquoise2 proteins were obtained from Dr. Michael Davidson (FSU, Tallahassee, FL). The mCerulean3 [8], mTurquoise [9], and mTurquoise2 [10] are engineered variants of mCerulean [11] with improved photophysical behavior. Standard recombinant DNA methods were used to generate the plasmids encoding the FRET standard proteins consisting of mCerulean3 linked to mVenus. Similar approaches were also used to generate the FPs linked in-frame to the sequence for the indicated proteins. All plasmid inserts were confirmed by direct sequencing. The purified FPs were provided by Dr. Michael Davidson and Paula Cranfill (FSU, Tallahassee, FL). The 6xHis-tagged proteins were grown in bacteria, which were disrupted by sonication, and the supernatant was recovered by centrifugation. The supernatant was mixed with Talon resin and eluted. The purified FPs were concentrated using an Amicon Ultra centrifugal filter (Millipore) in PBS (pH 7.4). About 100 μl of the concentrated solution was added to an eight-chambered coverglass for the FLIM measurements described below.

2.2. Tissue culture and transfection

The mouse pituitary GHFT1 cells are maintained in monolayer culture and harvested at 80% confluence [12]. The cells are washed with phosphate buffered saline (PBS), treated briefly with trypsin (0.05% in 0.53 mM EDTA), and recovered by centrifugation in culture medium containing serum. The cells are washed two times by centrifugation in Dulbecco's calcium-magnesium free PBS and resuspended in Dulbecco's calcium-magnesium free PBS with 0.1% glucose and 0.1 ng/ml BioBrene Plus (Applied Biosystems, Inc.) at a final concentration of approximately $1x10^7$ cells per ml. Exactly 400 μl of the cell suspension is

transferred to each 0.2 cm gap electroporation cuvette containing the plasmid DNA(s). For FRET studies involving independently expressed donor- and acceptor-labeled proteins, the amount of plasmid DNA encoding the donor- and the acceptor-labeled proteins was adjusted to favor acceptor expression, using a total of 10 μg of purified plasmid DNA per cuvette. The contents of the cuvettes are gently mixed, and then pulsed with 200 volts at a capacitance of 1200 microfarads in a BTX ECM 830 electroporator (Harvard Apparatus), yielding pulse durations of about 10 ms. The cells are immediately recovered from the cuvette and diluted in phenol red-free tissue culture medium containing serum. The suspension is transferred to sterile two well-chambered coverglass (Lab-Tek II, Thermo Scientific), which are placed in an incubator (37°C and 5% CO_2) prior to FLIM the following day.

2.3. FD FLIM measurements

The fluorescence lifetime measurements are made using the ISS Alba FastFLIM system (ISS Inc., Champagne, IL) coupled to an Olympus IX71 microscope equipped with a 60 X, 1.2 numerical aperture water-immersion objective lens. A Pathology Devices (Pathology Devices, Inc.) stage-top environmental control system maintains the temperature at 36° C and CO_2 at 5%. For FD FLIM using the cyan and yellow FPs the 5 mW 448 nm diode laser is modulated by the Alba FastFLIM system at a fundamental frequency of 10 MHz, with additional measurements at up to 13 sinusoidal harmonics (10–140 MHz). The modulated laser is coupled to the confocal scanning system, which is controlled by the VistaVision software (Build 143, ISS Inc., Champagne, IL). The fluorescence signals emitted from the specimen are routed by a 495 nm long pass beam splitter through the 530/43 nm (acceptor emission) and 480/40 (donor emission) band-pass emission filters, and the signals are detected using two identical avalanche photodiodes (APD). The phase delays and modulation ratios of the emission relative to the excitation are measured at each pixel of an image for each frequency.

The system is calibrated with 50 mM Coumarin 6 dissolved in ethanol (reference lifetime 2.5 ns; http://www.iss.com/resources/reference/data_tables/LifetimeDataFluorophores.html). A chambered coverglass with the dye sample is illuminated at sufficient laser power to achieve approximately 100,000 counts per second in the donor emission channel, and frame averaging is used to calibrate the software using the 2.5 ns reference sample. To verify the calibration, lifetime measurements are made of a second reference standard, 10 mM HPTS (8 - hydroxypyrene - 1,3,6 - trisulfonic acid from Santa Cruz Biotechnology, Inc.) dissolved in phosphate buffer (PB) pH 7.8 (reference lifetime of 5.3 ns [13]). The distribution of the lifetimes for all the pixels in the image is determined using the phasor (polar) plot method [14–19].

For live-cell FD FLIM measurements from transfected cells producing the FP-labeled proteins, the cells are first identified by epifluorescence microscopy. For FD FLIM measurement using the confocal laser scanning system and APD detectors, it is important to adjust the laser power to achieve a similar count rate in the donor emission channel to that used for calibration of the system. Frame averaging is used to acquire a 256 × 256 pixel lifetime image with about 200 peak counts per pixel. This typically requires about 45 seconds, and it is important to adjust laser power so that there is no significant photobleaching of the samples during image acquisition. The FLIM images are analyzed with the VistaVision software by selecting regions of interest (ROI, typically 1–2 μm^2) with average intensity > 75 counts. The most accurate lifetime determinations are obtained by analyzing the first 12 frequencies (10 – 120 MHz). The quality of the fit is judged by the reduced chi-square values for the Weber plots of phase delay and modulation ratio vs. frequency. The ratio of the donor lifetimes determined in the absence (τ_D) and in the

presence of the acceptor (τ_{DA}) provides a direct estimate of FRET efficiency (E_{FRET}) by Eq. 1:

$$E_{FRET}=1-\frac{\tau_{DA}}{\tau_{D}} \quad [1]$$

For intermolecular FRET measurements from independently expressed proteins, the ratio of the acceptor- to the donor-labeled proteins influences the E_{FRET} [19, 20]. The two-channel imaging system used here allows simultaneous measurement of the intensity of the donor emission (I_D) and the intensity of the acceptor emission (I_A), which are detected by the two identical APDs. The mean intensity in both the donor and the acceptor channels are measured for each ROI, and this serves as a proxy for the ratio of the acceptor- to the donor-labeled proteins in each ROI. The FRET efficiency is calculated using Eq. 1 from the lifetime of the quenched donor determined for each ROI, and the averaged results for each cell are plotted as a function of the measured acceptor to donor (I_A/I_D) ratio. The data are fitted by a nonlinear regression for saturation binding constraining the background to zero using the GraphPad Prism software.

3. Results and discussion

3.1. Lifetime measurement of purified FPs alone and in mixtures

The FD lifetime images are analyzed using the phasor plot method, which was originally developed as a way to analyze transient responses to repetitive experimental perturbations, and can be applied to any system with frequency characteristics [15, 16]. The phasor plot is a simple geometric representation of the relative modulation ratio (M) and the phase delay (φ) of the emission signal measured at every pixel in an image. The frequency characteristics of the emission signal from each image pixel is plotted on a polar coordinate system using a vector with length determined by the modulation ratio and angle determined by the phase delay. The phase delay and modulation ratio are related to the lifetime (τ) at particular frequency ω as:

$$\tau_{(\omega)}=\tan\phi \text{and} \tau_{(\omega)}={\sqrt{1}}/{\mathrm{M2}}-1$$

For a single exponential decay, the relationship M = cos φ describes a vector with an endpoint that falls on a universal semicircle with a radius of 0.5 that is centered at (0.5, 0) on the polar coordinate system. The semicircle is universal in the sense that the lifetime distribution for any species with a single-exponential decay will fall directly on the semicircle irrespective of the lifetime or modulation frequency [15, 16]. The X and Y intercepts of the vector correspond to the polar coordinates G = M cos φ and S = M sin φ, with longer lifetimes to the left (see Fig. 1). It is important to emphasize that this is a direct measurement of the fluorescence lifetime of the fluorophores within a specimen, and does not require fitting to determine the time decay parameters of the separate components [15–19].

To demonstrate the analysis of fluorescence lifetime measurements using the phasor plot method, FD FLIM was used to acquire images from solutions containing either the purified mCerulean or mTurquoise2 FPs, or mixtures of the two FPs. Turquoise2 is an engineered variant of Cerulean that retains the same spectral characteristics, but has a markedly improved quantum yield (0.93 vs. 0.49 for Cerulean) [10]. A direct consequence of the increased quantum yield of mTurquoise2 is a longer fluorescence lifetime compared to mCerulean [21]. The acquisition and analysis of FD FLIM data are demonstrated here using

the Weber plot (Fig. 1A) of the phase delay and modulation ratio for the purified mCerulean or mTurquoise2 samples measured at multiple frequencies. A phasor plot is then generated from the data obtained at 30 MHz, and this clearly shows the distinct lifetime distributions for mCerulean3 and mTurquoise2, with the distribution for the longer-lifetime mTurquoise2 shifted to the left along the universal semicircle (Fig. 1B).

The phasor analysis also provides important information about the photophysical behavior of the purified FPs. The lifetime distribution for mTurquoise2 lies slightly above the universal semicircle (Fig. 1B), which can be an indication of artifacts interfering with the measurements, including photobleaching events during acquisition [15]. Our data suggest that there is a small fraction of Turquoise2 that is sensitive to photobleaching. The analysis of data demonstrates that Turquoise2 is best fit by a single-exponential lifetime decay of 4.5 ns (Table 1). In contrast, the phasor plot for purified mCerulean falls inside the universal semicircle, and this is diagnostic for the presence of more than one lifetime component (Fig. 1B). The analysis of the data acquired for mCerulean shows it is best fit by a two-component decay, with lifetimes of 4.8 ns (34%) and 2.1 ns (66%), resulting in an intensity-weighted average lifetime of 3.1 ns (Table 1).

The distinct locations of the lifetime distributions for these two spectrally identical FPs on the polar coordinate system not only clearly identifies the spectrally identical species, but importantly, can also determine their relative contributions in mixtures. This is illustrated in the phasor analysis of mixtures of the purified mTurquoise2 and mCerulean (Fig. 1C). The lifetime distributions for each mixture are determined solely from the phase delay and modulation ratio of the emission signal from each image pixel. The lifetimes for the mixtures of purified proteins, determined from the phasor analysis are presented in Table 2. The locations of the lifetime distributions for each mixture on the phasor plot fall on a straight line that connects the distributions for the two different pure species, and the position on the line identifies the relative fraction of each lifetime component [15]. Together, these results demonstrate how the phasor plot analysis enables the separation of different lifetime components from FD FLIM images without the need for fitting algorithms.

3.2. FRET-FLIM measurements from FRET standard proteins

Next, the phasor analysis is applied to FD FLIM measurements from living cells expressing the “FRET standard” fusion proteins. The FRET standard approach that was developed by the Vogel laboratory provides a straightforward method to verify both the biological model, and the imaging system used for FRET measurements [22,23]. The original FRET standard fusion proteins consist of mCerulean linked to mVenus. However, since mCerulean has more than one lifetime (Fig. 1B, Table 1), it is replaced here by the mCerulean3 variant. The mCerulean3 FP has reduced photoswitching behavior and improved photostability compared to mCerulean, and the purified protein has a single component lifetime of 4.0 ns (Table 1) [8]. The plasmid encoding the fusion protein consisting of mCerulean3 coupled to mVenus through the five-amino acid (5aa) linker serves as a high FRET efficiency standard. Since the fluorescence lifetime can be very sensitive to the local environment of the donor fluorophore, a similar plasmid that encodes the mCerulean3 linked to mutant variant of mVenus, called Amber, was also generated. The mutation converts the chromophore tyrosine to a cysteine producing a non-fluorescent form of Venus that folds correctly, but does not act as a FRET acceptor [24]. Thus, the local environment for Cerulean3 is same for the Amber and Venus constructs, with the Cerulean3-5aa-Amber fusion protein providing an accurate measurement of the unquenched donor lifetime. Additionally, a fusion protein consisting of mCerulean3 linked to mVenus through the 229-amino acid tumor necrosis factor receptor associated factor (TRAF) domain (Cerulean3-TRAF-Venus) is used to provide a low FRET efficiency standard [23].

The composite phasor plot in Fig. 2 compares the unquenched and quenched donor lifetimes for the different Cerulean3 FRET standard fusion proteins expressed in living cells. The intensity images obtained from each of the cells expressing the different FRET standard fusion proteins are shown in the right panels of Fig. 2, with the ROI that was used to determine the average lifetime indicated. For the cell expressing Cerulean3-5aa-Amber (Fig. 2A), the unquenched donor lifetime was 3.96 ns, and was best fit as a single-component decay. The donor lifetime for the Cerulean3-TRAF-Venus fusion protein, determined in the indicated ROI (Fig. 2B) was 3.68 ns, corresponding to a FRET efficiency (E_{FRET}) of 7% (determined by Eq. 1). In contrast, the lifetime distribution for the cell expressing Cerulean3-5aa-Venus (Fig. 2C) clearly shows the quenched donor lifetime for this high FRET standard, and falls inside the semicircle, indicative of the multi-component lifetime. The multi-component lifetime for this genetic FRET construct comprised of one donor linked to one acceptor arises because the FPs rotate slowly relative to their fluorescence lifetime. Since there will be a negligible change in the dipole orientation during the excited state lifetime, little averaging will occur. Monte-Carlo simulations were recently used to demonstrate that the slow rotation of the FPs has the potential to give rise to a bimodal distribution of efficiencies in FRET experiments [24]. When analyzing the multi-exponential lifetimes that result from the linked FRET standard protein, the energy transfer efficiency is determined using the amplitude-weighted lifetime [21]. The amplitude-weighted lifetime for Cerulean3-5aa-Venus is 2.36 ns (Fig. 2C), which corresponds to an E_{FRET} of 40%.

3.3. Measuring the homologous interactions of the C/EBPα BZip domain by FRET-FLIM

The FD FLIM method is next applied to the detection of the homologous interactions between the basic region leucine zipper (BZip) domains of the transcription factor C/EBPα. The C/EBP transcription factors bind to DNA as obligate dimers through interactions between their BZip domains [25]. These transcription factors localize to regions of centromeric heterochromatin by binding to consensus DNA elements in repeated α-satellite sequences that are readily detected in mouse cells [26, 27]. Here, mouse pituitary GHFT1 cells expressing the C/EBPα BZip domain labeled with mTurquoise only (donor) or in combination with the BZip domain fused mVenus (acceptor) are imaged using FD FLIM (see Fig. 3A). The purified mTurquoise protein has a single component lifetime of 4.1 ns (Table 1), and behaves similarly to Cerulean3 as a donor fluorophore (Day and Davidson, in preparation). Representative intensity images of the nucleus of a cell that expressed only the mTurquoise BZip domain protein (donor alone, Fig. 3B), or the nucleus of a cell that co-expressed the mTurquoise- and Venus-BZip domain proteins (donor + acceptor, Fig. 3C) are shown. The areas of high fluorescence signal in the intensity images result from the localization of the BZip proteins to regions of centromeric heterochromatin in these mouse cells. The lifetime map in Fig. 3B depicts the unquenched donor lifetimes in regions of heterochromatin for mTurquoise-BZip domain expressed alone, indicated by warmer colors on the lookup table (LUT). In contrast, the quenched lifetimes of the Turquoise-BZip domain co-expressed with the Venus-labeled BZip domain, indicated by cooler colors on the LUT, are clearly seen in Fig. 3C.

The quantification of intermolecular FRET between labeled proteins independently produced in living cells requires several important considerations, illustrated here using the homologous interactions between the BZip domain proteins. First, the unquenched donor lifetime must be determined for the donor labeled proteins that are localized to the specific subcellular region. This is important since lifetime can be influenced by local environmental factors that may alter the excited state of the fluorophore. Here, the unquenched lifetime of the mTurquoise-BZip fusion protein bound to heterochromatin was measured in multiple different ROI within the nuclei of separate cells. The intensity images shown in Fig. 3B and 3C illustrate the areas of centromeric heterochromatin that are easily identified and selected

as individual ROI. For the measurement of unquenched donor lifetimes, separate regions are selected within each cell nucleus to determine the average lifetime for that cell. The measurements were then repeated for ten different cells, yielding an average lifetime for the mTurquoise-BZip proteins bound to heterochromatin of 3.84 ± 0.13 ns.

There are two important considerations regarding the donor-alone measurements. First, the FLIM analysis is greatly simplified when the donor FP has a single component lifetime, and, unlike mCerulean, the lifetime decay of mTurquoise is best fit to a single component (Table 1). Second, the donor-labeled proteins are interacting and forming dimers, so there will be energy migration FRET (homo-FRET) between the identical fluorophores. The homo-FRET process generally does not change the donor lifetime [28], but it was shown to shorten the lifetime of Cerulean [29]. The lifetime of mTurquoise (a freely diffusing monomer) measured in the cytoplasm of multiple cells was 3.82 ns ± 0.04, so it appears that homo-FRET is not quenching the mTurquoise-BZip proteins bound to heterochromatin.

The measurement of intermolecular FRET between the independently produced donor- and acceptor-labeled proteins requires additional considerations. Because the donor- and acceptor-labeled proteins are encoded by separate plasmids, each of the co-transfected cells will express a different ratio of the labeled proteins. The donor-to-acceptor ratio influences the E_{FRET}, since cells expressing predominately donor-labeled proteins will have little or no FRET, while cells with an excess of acceptor will have potentially high FRET [19, 20]. The lifetime imaging microscope used here is a two-channel system that simultaneously directs the emission signals through the donor (480/40 nm) and acceptor (530/43 nm) channels to the two identical APD detectors. There is no bleedthrough of the Venus (acceptor) emission signal into the donor channel, so measurement of the quenched donor lifetime (τ_{DA}) is all that is required for the determination of E_{FRET}. However, because the donor-to-acceptor ratio varies from cell to cell, it is necessary to determine the relative level of the donor- and acceptor-labeled proteins for each ROI that is selected for donor lifetime measurements. The mean intensity in both the donor (I_D) and the acceptor (I_A) channels are measured for each of the ROI used for lifetime determination, and this serves as a proxy for the ratio of the acceptor- to the donor-labeled proteins in each ROI, providing a straightforward and consistent approach to qualitatively determine the relative expression of the donor and acceptor labeled proteins. The measurement of the quenched donor lifetime in the same ROI allows the determination of E_{FRET} (Eq. 1) at a particular (I_A/I_D) ratio.

The results in Fig. 3D show the relationship of the E_{FRET} determined by fluorescence lifetime for the mTurquoise-BZip domain co-expressed with the mVenus-BZip domain protein when plotted as a function of the different I_A/I_D ratios. The average I_A/I_D ratio (± SD) and the average E_{FRET} (± SD) are represented for multiple cells across a range of I_A/I_D (Fig. 3D). As the acceptor to the donor ratio is increased, there is more quenching of the mTurquoise-BZip donor signal (detected in the 480/40 nm donor channel). The highest E_{FRET} values (lowest donor lifetimes) are achieved in cells where the mVenus-BZip domain is in excess so that the maximum number of mTurquoise-BZip domain proteins is paired with the acceptor-labeled protein. A further increase in the mVenus-BZip domain proteins will not change FRET efficiency. The data are fitted by a nonlinear regression for saturation binding intersecting zero, since without the acceptor there can be no FRET (i.e., the unquenched donor). The results in Fig. 3D demonstrate that the E_{FRET} for the BZip protein interaction plateaus at high I_A/I_D ratios.

3.4. Measuring heterologous protein interactions in living cells using FRET-FLIM

The heterochromatin protein 1 (HP1) family proteins are highly conserved non-histone proteins that recognize the methylated lysine 9 of histone H3 [30, 31]. While the role of the HP1 proteins in directing the assembly and maintenance of heterochromatin is well

established, it has become increasingly clear that HP1 also plays roles in the regulation of gene expression [32]. In this regard, the interactions between HP1α and C/EBPα, a transcription factor involved in the control of cellular differentiation [25] is of significant interest. In earlier studies, we demonstrated that HP1α and C/EBPα interact when the proteins are bound to heterochromatin [33], and that only the BZip domain of C/EBPα was necessary for the interaction with HP1α [34]. Here, the FRET-FLIM approach is used to quantify the heterologous protein interactions between BZip domain of C/EBPα and HP1α.

First, the lifetime for the BZip domain labeled with Turquoise was determined in regions of heterochromatin (typically five to ten ROI per cell nucleus) for ten different cells, yielding an average unquenched donor lifetime of 3.89 ± 0.08 ns. Then intensity images and lifetime measurements were made from cells co-producing the mTurquoise-BZip domain proteins and Venus-HP1α (Fig. 4A). As a control for non-specific signals, measurements were also made from cells producing the mTurquoiseN1 protein (localized in both cytoplasm and nucleus) and Venus-HP1α (nuclear, see Fig. 4B). The lifetime map in Fig. 4B demonstrates the quenched lifetimes of the Turquoise-BZip domain co-expressed with the Venus-labeled HP1α, indicated by cooler colors on the LUT. In contrast, the lifetime of the TurquoiseN1 protein was not changed when co-expressed with Venus-HP1α (Fig. 4B, 4C). The E_{FRET} was then determined for cell co-producing mTurquoise-BZip domain proteins and Venus-HP1α with different I_A/I_D ratios (Fig. 4C). This result clearly shows that the BZip domain of C/EBPα is sufficient for the interaction with HP1α. To demonstrate that this dependence of E_{FRET} on the I_A/I_D ratio was not the result of background signals (such as crosstalk from the acceptor) detected in the donor channel, the nuclear localized mVenus-HP1α was co-produced with mTurquoiseN1 protein. Here, there was no trend toward increased E_{FRET} with increasing I_A/I_D ratio (Fig. 4C).

4. Concluding remarks

The relevance of the transient interactions between proteins inside living cells depends on the context in which they occur. In this regard, the continued development of non-invasive quantitative imaging techniques to visualize these protein interactions is critical for understanding how networks of PPI form inside intact cells. While the high-throughput approaches of yeast two-hybrid and co-affinity purification followed by mass spectrometry do the heavy lifting for the mapping of interactomes, verification and fine-tuning is necessary using many different types of cellular assays. The non-invasive FRET-FLIM imaging approach described here provides a quantitative approach to interrogate PPI in living cells. The phasor plot analysis of the fluorescence lifetime of the fluorophores within a specimen is a direct measurement that does not require fitting to determine the time decay parameters of the separate components [15–19].

A limitation of the FRET-FLIM approach is the necessity of producing the exogenous proteins of interest labeled with the FPs inside living cells. It is critical to verify that the FP-labeled proteins retain the functions of the endogenous proteins. Furthermore, the overexpression of some FP-labeled proteins may interfere with the cellular processes that are to be measured. This is a general concern that is shared with many different types of assays, and requires careful control experiments. The FPs described here have been extensively modified through mutagenesis to optimize their characteristics for expression and imaging in living cells. The many new FP probes are allowing non-invasive imaging techniques to complement and extend the results that are obtained by the biochemical analysis of the endogenous cellular proteins. Importantly, the measurements obtained from proteins labeled with the FPs in the natural environment inside living cells provide the most physiologically relevant information about protein behavior currently available.

Acknowledgments

This research was supported in part by NIH 2RO1 DK43701, 3RO1 DK43701-15S1, and the Indiana University School of Medicine (RND). The author thanks Dr. Michael Davidson and Paula Cranfill for the plasmids encoding the fluorescent proteins and the purified proteins.

References

1. Baker M. Nature. 2012; 484:271–275. [PubMed: 22498631]
2. Cusick ME, Klitgord N, Vidal M, Hill DE. Human molecular genetics. 2005; 14(Spec No. 2):R171–R181. [PubMed: 16162640]
3. Venkatesan K, Rual JF, Vazquez A, Stelzl U, Lemmens I, Hirozane-Kishikawa T, Hao T, Zenkner M, Xin X, Goh KI, Yildirim MA, Simonis N, Heinzmann K, Gebreab F, Sahalie JM, Cevik S, Simon C, de Smet AS, Dann E, Smolyar A, Vinayagam A, Yu H, Szeto D, Borick H, Dricot A, Klitgord N, Murray RR, Lin C, Lalowski M, Timm J, Rau K, Boone C, Braun P, Cusick ME, Roth FP, Hill DE, Tavernier J, Wanker EE, Barabasi AL, Vidal M. Nature methods. 2009; 6:83–90. [PubMed: 19060904]
4. Kocher T, Superti-Furga G. Nature methods. 2007; 4:807–815. [PubMed: 17901870]
5. Cusick ME, Yu H, Smolyar A, Venkatesan K, Carvunis AR, Simonis N, Rual JF, Borick H, Braun P, Dreze M, Vandenhaute J, Galli M, Yazaki J, Hill DE, Ecker JR, Roth FP, Vidal M. Nature methods. 2009; 6:39–46. [PubMed: 19116613]
6. Perez-Bercoff A, Hudson CM, Conant GC. PloS one. 2013; 8:e52581. [PubMed: 23320073]
7. Nagai T, Ibata K, Park ES, Kubota M, Mikoshiba K, Miyawaki A. Nat Biotechnol. 2002; 20:87–90. [PubMed: 11753368]
8. Markwardt ML, Kremers GJ, Kraft CA, Ray K, Cranfill PJ, Wilson KA, Day RN, Wachter RM, Davidson MW, Rizzo MA. PloS one. 2011; 6:e17896. [PubMed: 21479270]
9. Goedhart J, van Weeren L, Hink MA, Vischer NO, Jalink K, Gadella TW Jr. Nature methods. 2010; 7:137–139. [PubMed: 20081836]
10. Goedhart J, von Stetten D, Noirclerc-Savoye M, Lelimousin M, Joosen L, Hink MA, van Weeren L, Gadella TW Jr, Royant A. Nature communications. 2012; 3:751.
11. Rizzo MA, Springer GH, Granada B, Piston DW. Nat Biotechnol. 2004; 22:445–449. [PubMed: 14990965]
12. Lew D, Brady H, Klausing K, Yaginuma K, Theill LE, Stauber C, Karin M, Mellon PL. Genes Dev. 1993; 7:683–693. [PubMed: 8096199]
13. Ryder AG, Glynn TJ, Przyjalgowski MA, Szczupak BA. Journal of Fluorescence. 2002; 12:177–180.
14. Colyer RA, Lee C, Gratton E. Microscopy research and technique. 2008; 71:201–213. [PubMed: 18008362]
15. Redford GI, Clegg RM. J Fluoresc. 2005; 15:805–815. [PubMed: 16341800]
16. Jameson DM, Gratton E, Hall RD. Applied spectroscopy reviews. 1984; 20:55–106.
18. Hinde E, Digman MA, Welch C, Hahn KM, Gratton E. Microscopy research and technique. 2012; 75:271–281. [PubMed: 21858900]
19. Sun Y, Hays NM, Periasamy A, Davidson MW, Day RN. Methods in enzymology. 2012; 504:371–391. [PubMed: 22264545]
20. Chen H, Puhl HL 3rd, Koushik SV, Vogel SS, Ikeda SR. Biophys J. 2006; 91:L39–L41. [PubMed: 16815904]
21. Lakowicz, JR. Principles of fluorescence spectroscopy. 3rd ed.. New York: Springer; 2006.
22. Thaler C, Koushik SV, Blank PS, Vogel SS. Biophys J. 2005; 89:2736–2749. [PubMed: 16040744]
23. Koushik SV, Chen H, Thaler C, Puhl HL 3rd, Vogel SS. Biophys J. 2006; 91:L99–L101. [PubMed: 17040988]
24. Vogel SS, Nguyen TA, van der Meer BW, Blank PS. PloS one. 2012; 7:e49593. [PubMed: 23152925]

25. Ramji DP, Foka P. The Biochemical journal. 2002; 365:561–575. [PubMed: 12006103]
26. Tang QQ, Lane MD. Genes Dev. 1999; 13:2231–2241. [PubMed: 10485846]
27. Day RN, Periasamy A, Schaufele F. Methods. 2001; 25:4–18. [PubMed: 11558993]
28. Levitt JA, Matthews DR, Ameer-Beg SM, Suhling K. Current opinion in biotechnology. 2009; 20:28–36. [PubMed: 19268568]
29. Koushik SV, Vogel SS. Journal of biomedical optics. 2008; 13:031204. [PubMed: 18601528]
30. Bannister AJ, Zegerman P, Partridge JF, Miska EA, Thomas JO, Allshire RC, Kouzarides T. Nature. 2001; 410:120–124. [PubMed: 11242054]
31. Lachner M, O'Carroll D, Rea S, Mechtler K, Jenuwein T. Nature. 2001; 410:116–120. [PubMed: 11242053]
32. Kwon SH, Florens L, Swanson SK, Washburn MP, Abmayr SM, Workman JL. Genes Dev. 2010; 24:2133–2145. [PubMed: 20889714]
33. Demarco IA, Periasamy A, Booker CF, Day RN. Nature methods. 2006; 3:519–524. [PubMed: 16791209]
34. Siegel AP, Hays NM, Day RN. Journal of biomedical optics. 2013; 18:25002. [PubMed: 23392382]

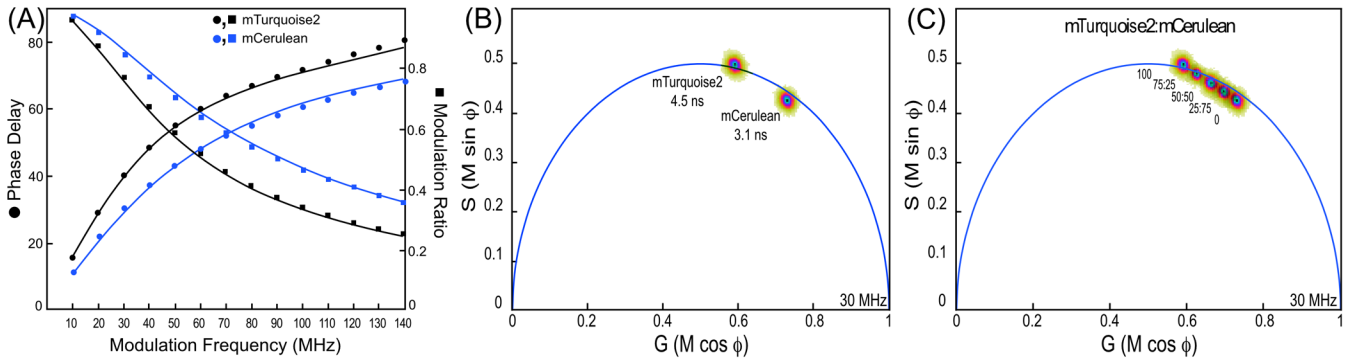

Fig. 1.

FLIM measurements of purified mTurquoise2 and mCerulean. (A) The Weber plot demonstrates the analysis of the multi-frequency (10–140 MHz) measurements of phase delay and modulation ratio obtained from the samples of purified mTurquoise2 and mCerulean. (B) The composite phasor plot for the measurements of the lifetime distributions for mTurquoise2 or mCerulean obtained at the frequency of 30 MHz. The analysis of the distributions yields a single component lifetime of 4.5 ns for mTurquoise2, and a two-component intensity-weighted average lifetime of 3.1 ns for mCerulean. (C) The composite phasor plot for the measurements of the lifetime distributions for mixtures of mTurquoise2 and mCerulean obtained at the frequency of 30 MHz.

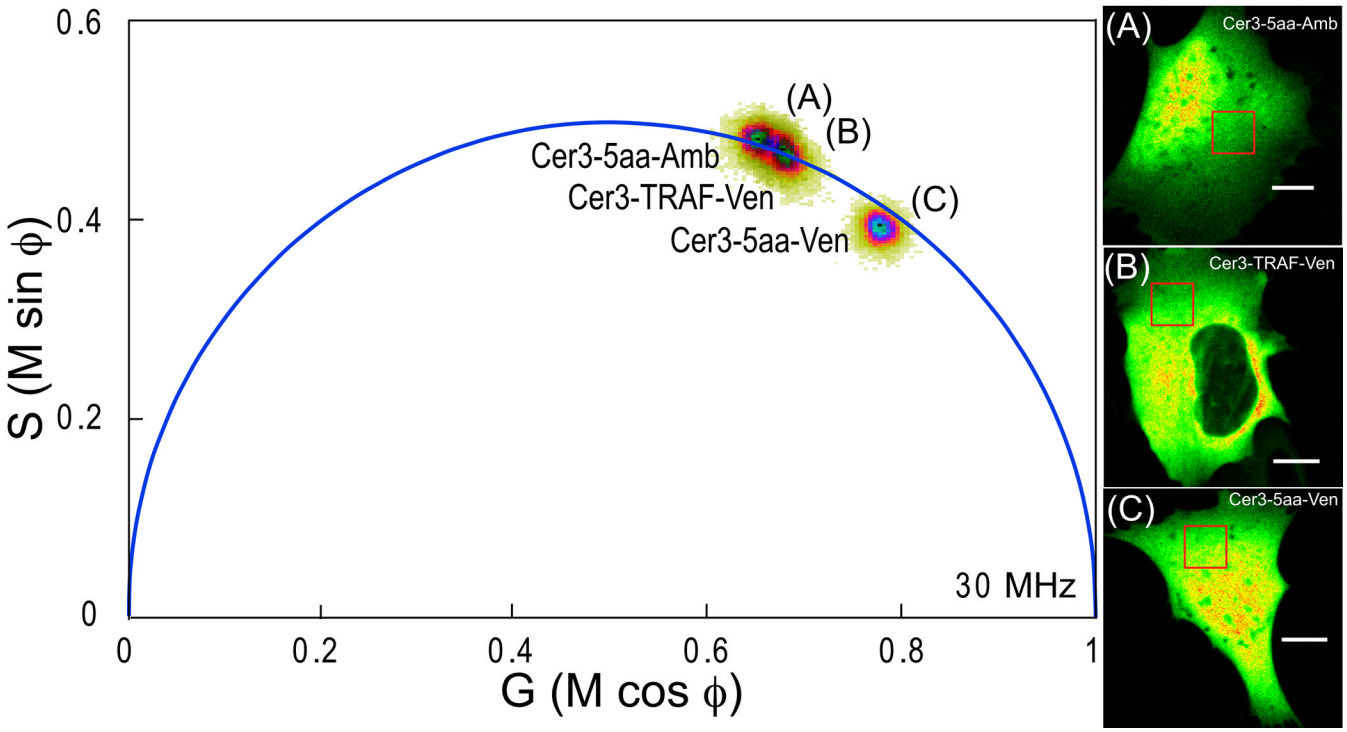

Fig. 2.

The phasor plot analysis of the lifetimes determine for the Cerulean3 FRET standards produced in living cells. (A) The phasor lifetime distribution and intensity image of a cell expressing Cerulean3-5aa-Amber (unquenched donor). The lifetime distribution on the phasor plot represents every pixel in the image, and the intensity-weighted average lifetime of 3.96 ns was determined in the ROI indicated by the red box in the intensity image; the calibration bar indicates 10 μm. (B) The phasor lifetime distribution and intensity image of a cell expressing Cerulean3-TRAF-Venus. The average lifetime of 3.68 ns was determined in the indicated ROI. (C) The phasor lifetime distribution and intensity image of a cell expressing Cerulean3-5aa-Venus. The amplitude-weighted average lifetime of 2.36 ns was determined in the indicated ROI.

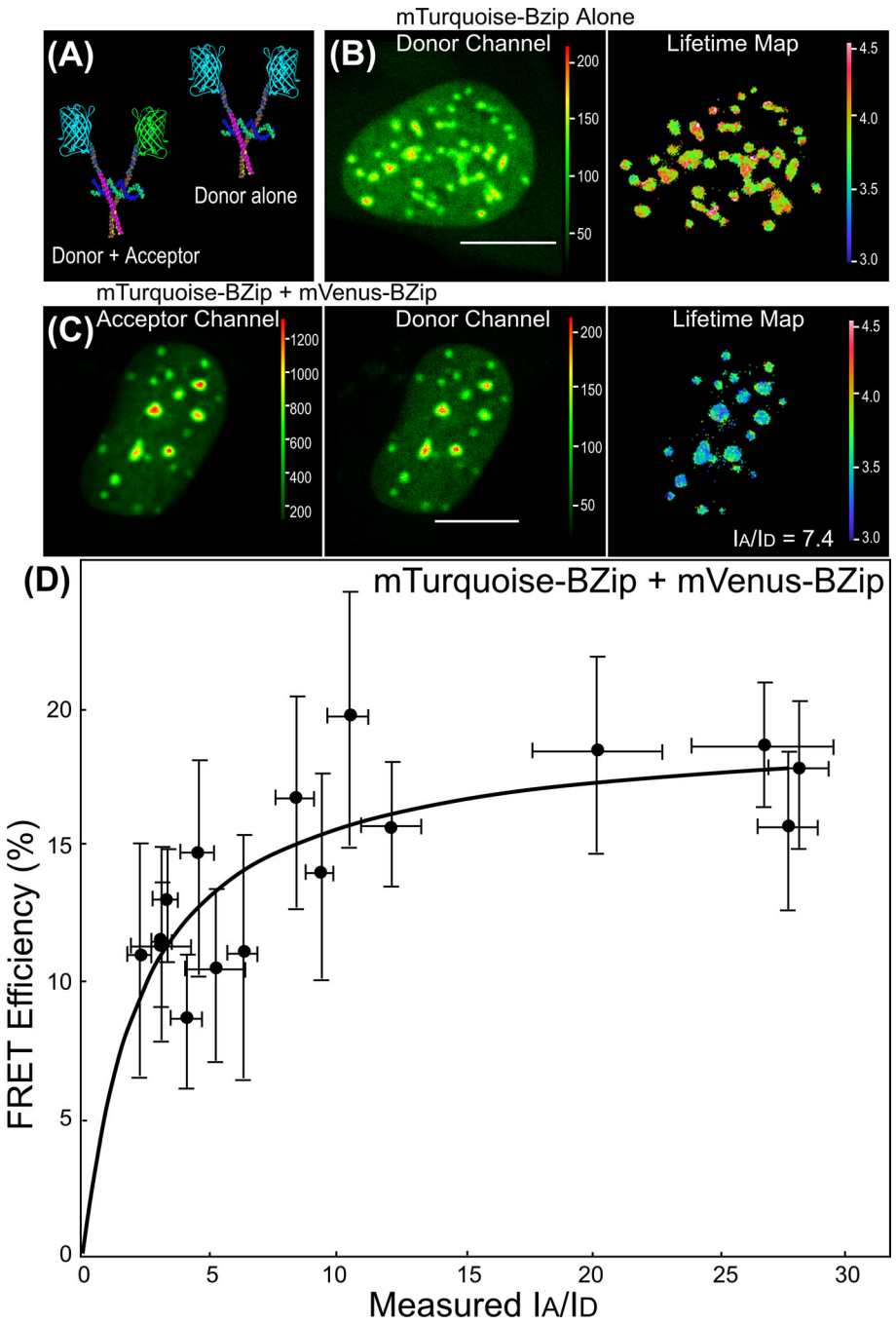

Fig. 3.

FRET-FLIM analysis of the homologous interactions between C/EBPα BZip domain proteins. (A) A diagrammatic representation of the mTurquoise-labeled BZip (donor alone) or the co-expressed mTurquoise-and mVenus-labeled BZip domain proteins (donor + acceptor) bound to DNA as obligate dimers. (B) The intensity image from the donor channel and the lifetime map for the nucleus of a cell expressing only the mTurquoise-BZip domain (donor alone); the calibration bar indicates 10 μm. (C) The intensity images for the nucleus of a cell expressing both the mTurquoise- and mVenus-BZip domain (donor + acceptor) acquired in the acceptor channel, donor channel, and the lifetime map at an I_A/I_D ratio of 7.4. (D) FLIM was used to measure the donor lifetime in multiple ROI for each cell, and the

FRET efficiency (%) was determined from the averaged donor lifetime using Eq. 1. The results are plotted as a function of average I_A/I_D measured from each cell. Each point represents the average E_{FRET} (± SD) at the average I_A/I_D (± SD) for multiple ROI from an individual cell.

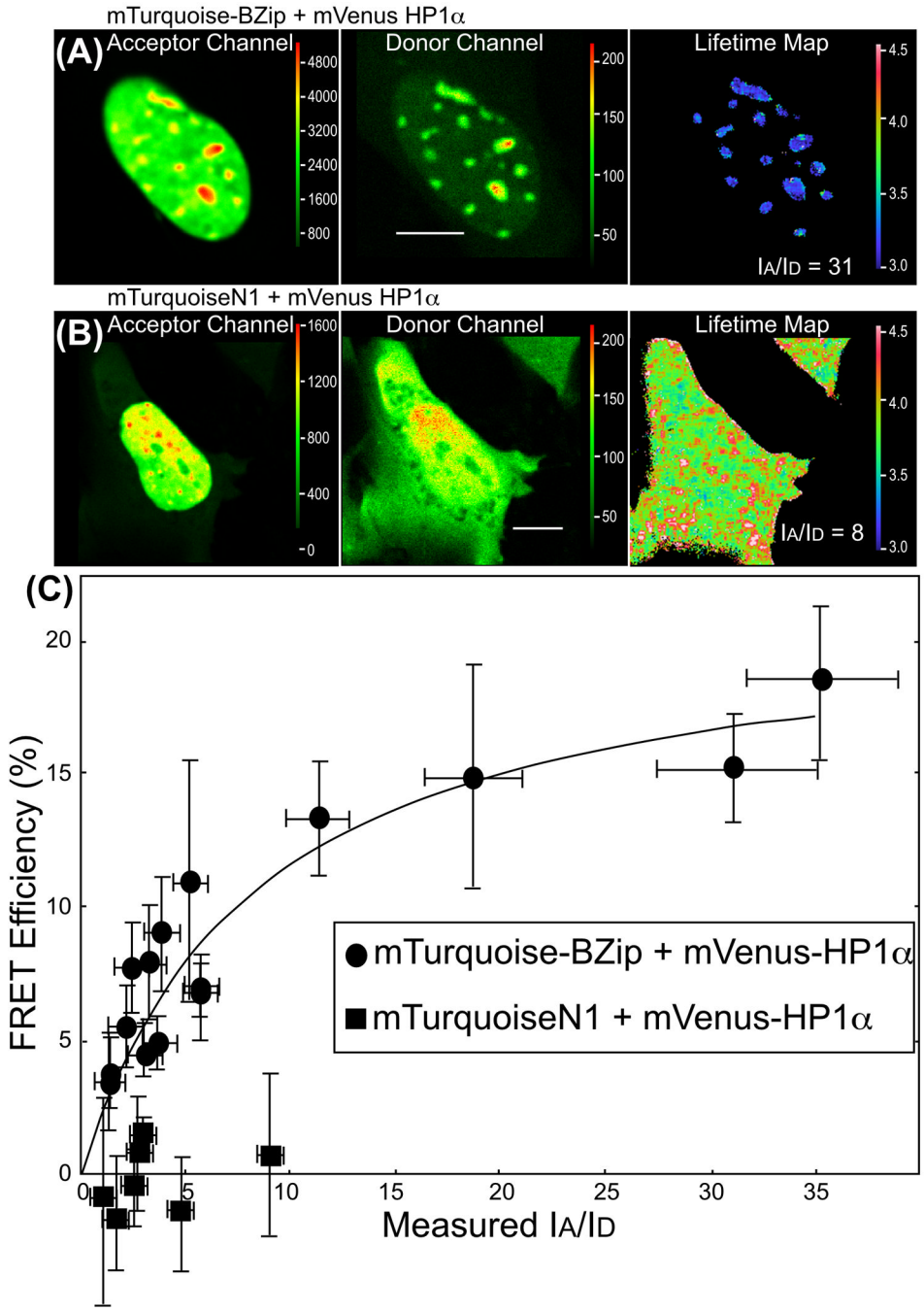

Fig. 4.

FRET-FLIM analysis of the heterologous interactions between the C/EBPα BZip domain and HP1α. (A) The intensity images for the nucleus of a cell expressing both the mTurquoise-BZip domain and mVenus-HP1α acquired in the acceptor channel, donor channel (the calibration bar indicates 10 μm), and the corresponding lifetime map for the cell with an I_A/I_D ratio of 31. (B) The intensity images for a cell expressing both the mTurquoiseN1 (localized throughout the cytoplasm and nucleus) and mVenus-HP1α (nuclear) acquired in the acceptor channel, donor channel, and the corresponding lifetime map for the cell with an I_A/I_D ratio of 8. (C) FLIM was used to measure the donor lifetime in multiple ROI for each cell, and the FRET efficiency (%) was determined. Each point

represents the average E_{FRET} (± SD) at the average I_A/I_D (± SD) for multiple cells expressing the indicated donor- and acceptor-labeled proteins.

Table 1

FD FLIM analysis of the purified protein variants of Cerulean.

Fluorescent Protein[a]	2-component lifetime (Fraction) [b]	Tau(f)[c] (± SD)	R_0 Venus[d] (Å)
Cerulean	2.1 ns (0.66) 4.8 ns (0.34)	3.1 ± 0.03	50
Cerulean3	4.0 ns (0.99)	4.0 ± 0.02	54
Turquoise	4.1 ns (0.99)	4.1 ± 0.01	55
Turquoise2	4.4 ns (0.99)	4.4 ± 0.04	56

[a] Purified proteins, n = 3.

[b] Measurements were made at 12 frequencies from 10 to 120 MHz.

[c] Tau(f) is the intensity-weighted average lifetime.

[d] Förster distance determined by: $R_0 = 0.211\ [(\kappa^2)(n^{-4})\ (QY_D)\ (J_\lambda)]^{1/6}$

Table 2

FD FLIM analysis of mixtures of the purified Cerulean and Turquoise2.

Fluorescent Protein mixture[a]	2-component lifetime (Fraction) [b]	Tau(f)[c] (± SD)
Cerulean (100)	2.5 ns (0.65)	3.2
Turquoise2 (0)	4.7 ns (0.35)	
Cerulean (75)	3.2 ns [d] (0.76)	3.4
Turquoise2 (25)	4.6 ns (0.23)	
Cerulean (50)	3.2 ns [d] (0.51)	3.8
Turquoise2 (50)	4.6 ns (0.49)	
Cerulean (25)	3.2 ns [d] (0.24)	4.2
Turquoise2 (75)	4.6 ns (0.76)	
Turquoise2 (0)	4.6 ns (1)	4.6

[a] Mixed at indicated ratio to yield 10^5 counts in 300 μL PBS, n = 1.

[b] Measurements were made at 12 frequencies from 10 to 120 MHz.

[c] Tau(f) is the intensity-weighted average lifetime.

[d] Lifetimes fixed, fraction unconstrained.